*Human Molecular Genetics*, 2016, Vol. 25, No. 7 1345–1356

**doi: 10.1093/hmg/ddw017**
Advance Access Publication Date: 24 January 2016
Original Article

ORIGINAL ARTICLE

# Loss of human disease protein retinitis pigmentosa GTPase regulator (RPGR) differentially affects rod or cone-enriched retina

Kollu N. Rao[1], Linjing Li[1], Wei Zhang[1], Richard S. Brush[2], Raju V.S. Rajala[2] and Hemant Khanna[1,*]

[1]Department of Ophthalmology, University of Massachusetts Medical School, 368 Plantation St, Albert Sherman Center AS6-2043, Worcester, MA 01605, USA and [2]University of Oklahoma Health Sciences Center, Oklahoma City, OK 73104, USA

*To whom correspondence should be addressed. Tel: +1 5088568991; Fax: +1 5088561552; Email: hemant.khanna@umassmed.edu

## Abstract

It is unclear how genes, such as *RPGR* (retinitis pigmentosa guanine triphosphatase regulator) that are expressed in both rods and cones, cause variable disease pathogenesis. Using transcriptomic analysis, we show that loss of RPGR in a rod-dominant mouse retina ($Rpgr^{ko}$) results in predominant alterations in genes involved in actin cytoskeletal dynamics, prior to onset of degeneration. We validated these findings and found an increase in activated RhoA-GTP levels and polymerized F-actin in the $Rpgr^{ko}$ mouse retina. To assess the effect of the loss of RPGR in the all-cone region of the human retina, we used $Nrl^{-/-}$ (neural retina leucine zipper) mice, to generate $Rpgr^{ko}$::$Nrl^{-/-}$ double-knock-out (*Rpgr*-DKO) mice. These mice exhibited supranormal cone response to light and substantially retained retinal architecture. Transcriptomic analysis revealed predominant up-regulation of retinal pigmented epithelium (RPE)-specific genes associated with visual cycle, whereas fatty acid analysis showed mild decrease in docosahexaenoic acid in the retina of the *Rpgr*-DKO mice when compared with the $Nrl^{-/-}$ mice. Our data reveal new insights into distinct intracellular pathways that are involved in RPGR-associated rod and cone dysfunction and provide a platform to design new treatment modalities.

## Introduction

Our vision starts with detection of photons of light by photoreceptors (rods and cones). These neurons form the bulk of the retinal cell types and, along with the overlaying RPE, comprise the light-sensing compartment of the eye (1). Photoreceptors are polarized neurons with a distinct sensory outer segment (OS; also called sensory cilium) and an inner segment involved in protein synthesis and transport (2,3). The OS is loaded with photopigment opsin (rod opsin in rods and cone opsin in cones), which binds to the chromophore to carry out light detection cascade. RPE is involved in regulating visual cycle by participating in the regeneration of the chromophore and OS maintenance (4–6). Vision loss due to degeneration and dysfunction of photoreceptors typically involves malfunction of the OS or the RPE. As cones are responsible for the bulk of our day vision, cone degeneration would eventually lead to legal blindness.

Retinitis pigmentosa (RP) is an inherited form of neurodegenerative retinal disease that affects ~1 in 3000 individuals (7). While RP is clinically and genetically heterogeneous, it is characterized by progressive loss of rod function and night blindness followed by cone loss and complete blindness, usually by the third decade of life (8,9). RP can be inherited in an autosomal dominant, autosomal recessive or X-linked manner. Of these, X-linked RP (XLRP) is the most severe and prevalent form of RP. Mutations in two genes, retinitis pigmentosa guanine triphosphatase (GTPase) regulator (*RPGR*) and *RP2* account for >90% of

**Received:** October 2, 2015. **Revised and Accepted:** January 18, 2016

XLRP cases (10,11). *RPGR* mutations are the most common cause of XLRP, accounting for >70% of XLRP cases and ~15% of simplex (isolated) RP cases (12,13). RPGR-associated disease shows variable degrees of severity with respect to early involvement of either rods or cones in males (14,15); some female carriers are also known to develop a relatively severe form of the disease (16). *RPGR* mutations are also associated with cone degeneration and macular atrophy (17,18), indicating predominantly cone dysfunction in the cone-rich region of the retina called the macula.

The *RPGR* gene encodes multiple alternatively spliced isoforms, of which there are two major isoforms: the constitutive isoform, which contains 19 exons (RPGR$^{1-19}$) and ORF15 isoforms containing 15 exons terminating in intron 15 (RPGR$^{ORF15}$) (19–24). RPGR is implicated in regulating protein trafficking in photoreceptors (22,25,26). The *Rpgr*$^{ko}$ mouse undergoes progressive retinal degeneration and mis-trafficking of opsins in photoreceptors (27). Naturally occurring mouse and canine models of *RPGR* mutations as well as additional gene-targeted mouse mutants of *Rpgr* have been reported (28–30). These models exhibit distinct rod and cone alterations as observed in patients.

Given discordant rod and cone involvement in RPGR-XLRP; here, we present our findings of the discordant effect of the loss of RPGR on rod-dominant or cone-only rodent retinas. Our studies not only provide new platforms to assess human cone disease in RP, but will also assist in developing targeted therapeutic strategies.

## Results

### Photoreceptor dysfunction and transcriptomic analysis of *Rpgr*$^{ko}$ in a rod-dominant background

To assess the pathogenic mechanism of the loss of *Rpgr*, we wanted to select an age of mice that is prior to any detectable photoreceptor dysfunction. Therefore, we analyzed the photoreceptor function in the *Rpgr*$^{ko}$ mice by electroretinography (ERG). Although such studies have been reported (27), we aimed to assess the photoreceptor dysfunction using similar conditions in all our experiments. While 8-month-old *Rpgr*$^{ko}$ mice show decreased rod (scotopic) and cone (photopic) responses (Fig. 1A and B) and decrease in the thickness of the outer nuclear layer (ONL; photoreceptor nuclei) (Fig. 1C) when compared with the wild-type (WT) counterpart, no effect was observed at 1 month of age. Therefore, we selected this age for further analysis.

To examine the effect of the loss of RPGR in a rod-dominant retina, we performed RNAseq analysis from three biological replicates of 1-month-old WT and *Rpgr*$^{ko}$ mouse retinas followed by differential gene expression analysis. Significantly differentially expressed genes were selected based on a cutoff of at least 2-fold change in the expression level between the two groups and false discovery rate (FDR) <0.05. Our analysis identified 132 differentially expressed transcripts that were annotated (Supplementary Material, Table S1). Bioinformatics analysis using ingenuity pathway analysis (IPA) and Database for Annotation,

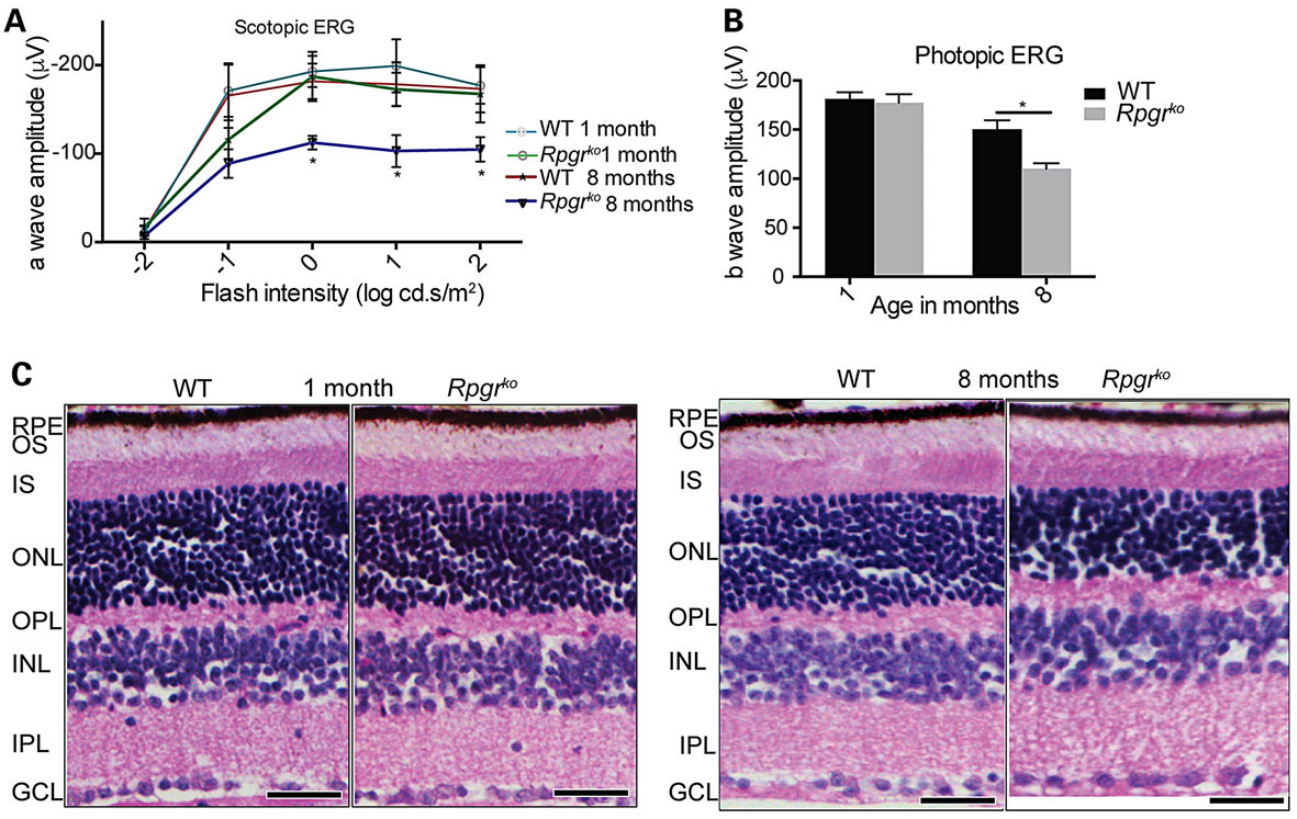


**Figure 1.** Phenotypic analysis of Rpgr$^{ko}$ mice. (**A** and **B**) ERG was performed using WT and *Rpgr*$^{ko}$ mice at indicated ages to examine Rod response (scotopic; A) at indicated flash intensities of light; and (B) cone response (photopic). *$P < 0.012$ (*t*-test). Ten mice of each genotype were analyzed for each experiment. (**C**) Histological analysis using hematoxylin-–eosin-stained paraffin sections of WT and *Rpgr*$^{ko}$ mice (10 mice) revealed decrease in the thickness of the ONL (photoreceptor nuclei) at 8 months of age whereas 1 month of age exhibited no appreciable difference. RPE: retinal pigment epithelium; OS: outer segment; IS: inner segment; OPL: outer plexiform layer; INL: inner nuclear layer; IPL: inner plexiform layer; GCL: ganglion cell layer. Scale: 50 μm.

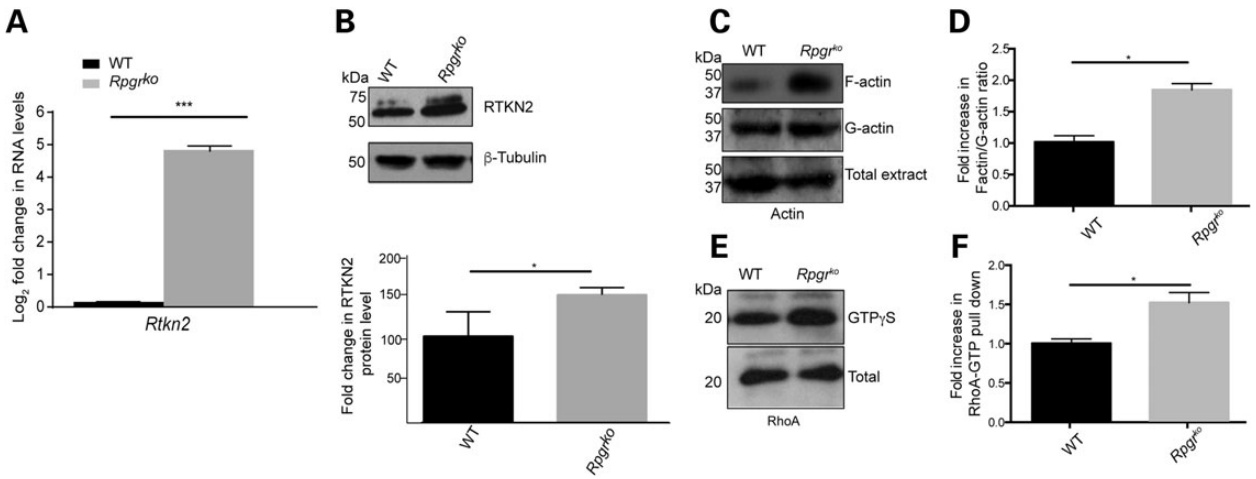


**Figure 2.** Actin cytoskeletal defects in the Rpgr$^{ko}$ mice.(**A**) qRT-PCR analysis of R*tkn2* was performed using 1-month-old WT or *Rpgr*$^{ko}$ retinas. The data are representative of three biological replicates. ***$P < 0.001$. (**B**) Protein extracts from WT and *Rpgr*$^{ko}$ retinas were analyzed by SDS–PAGE and immunoblotting using anti-RTKN2 or β-tubulin (loading control) antibody. Apparent molecular-weight markers are shown in kilodaltons (kDa). Relative band intensity is shown in the lower panel (*$P < 0.05$). (**C**) F- and G-actin fractions of the WT and the *Rpgr*$^{ko}$ mice (six each) were analyzed by SDS–PAGE and immunoblotting using the anti-actin antibody. Total protein extract was used as control for an equal amount of actin in the two samples. Apparent molecular-weight markers are shown in kilodaltons (kDa). The experiment was repeated three times. (**D**) Fold change in the ratio of F- to G-actin is represented, as measured by the band intensity of the anti-actin immunoreactive band in the F- or G-actin fractions of the WT and *Rpgr*$^{ko}$ mice (*$P < 0.05$). (**E**) Protein extracts from WT and *Rpgr*$^{ko}$ mice were prepared in the presence of non-hydrolyzable GTPγS and subjected to GST-pulldown using GST-RTKN fusion protein. The proteins were analyzed by immunoblotting using anti-RhoA antibody. Lower panel shows the total RhoA amount in the two extracts. Apparent molecular weight markers are shown in kilodaltons (kDa). (**F**) Graph represents fold change in the band intensity of RhoA-GTP pulled down by GST-RTKN in the WT versus *Rpgr*$^{ko}$ retina.

Visualization and Integrated Discovery, v6.7 (DAVID) identified five major categories of disrupted cellular functions: molecular transport, small-molecule biochemistry, cellular function and maintenance, cellular movement and cellular assembly and organization (Supplementary Material, Table S2). Among the cellular functions specific to the retina, we identified: cell death and survival, cellular assembly and organization, cellular function and maintenance, cell-to-cell signaling and interaction and cell morphology (Supplementary Material, Table S3). Further examination of the transcriptomics data revealed differential regulation of genes involved in actin cytoskeletal dynamics and in human diseases. As actin defects were implicated in RPGR-associated ciliary dysfunction in a previous study using *in vitro* cell culture model (31), we selected this pathway for further analysis. We validated the expression of three genes implicated in actin dynamics: STARD13 (StAR-related lipid-transfer domain protein 13), RTKN2 (Rhotekin 2) and SRPX (sushi-repeat containing protein, X-linked). STARD13 regulates RhoA and is involved in regulating cell adhesion mediated by actin cytoskeleton (32). RTKN2, on the other hand, is an effector of Rho GTPases, which binds to the activated form of Rho GTPases (33,34). SRPX was previously implicated in XLRP (35) and was also found to associate with the actin cytoskeleton (36). We validated the changes in the expression of *Rtkn2*, *Stard13* and *Srpx* by quantitative polymerase chain reaction (qPCR). Consistent with our RNAseq data, we detected a ~3.8-folds increase in the expression of *Stard13* and >25-folds increase in *Rtkn2* transcript levels in the *Rpgr*$^{ko}$ mice (Fig. 2A; Supplementary Material, Fig. S1A). On the other hand, *Srpx* expression was undetectable in the *Rpgr*$^{ko}$ retina.

## Actin cytoskeletal defects in *Rpgr*$^{ko}$ mice

Actin dynamics is associated with syndromic ciliopathies, including Bardet–Biedl syndrome (BBS) and is implicated in regulating cilia length (37,38). Moreover, actin filaments are localized at the base of the OS and are implicated in disc morphogenesis (39). To gain further insight into the status of actin cytoskeleton in the *Rpgr*$^{ko}$ retina, we first validated the changes in the protein level of RTKN2 protein in the retina. Immunoblot analysis of WT and *Rpgr*$^{ko}$ retinal extracts revealed a significant increase in the levels of the RTKN2 protein (Fig. 2B). As RTKN2 is involved in regulating polymerization of actin, we then calculated the ratio between polymerized filamentous (F)-actin and the globular (G)-actin in the 1-month-old WT and *Rpgr*$^{ko}$ retinas. By fractionating the retina followed by immunoblot analysis using anti-actin antibody, we found a 2-fold increase in the F- to G-actin ratio in the *Rpgr*$^{ko}$ retina when compared with the WT retina (Fig. 2C and D). No change in total actin levels was observed.

RhoGTPases are involved in the regulation of actin dynamics and increase in RhoA-GTP results in increased actin polymerization (40,41). We, therefore, hypothesized that increased levels of polymerized actin in the *Rpgr*$^{ko}$ retina are associated with higher RhoA-GTP levels. Effectors of small GTPases recognize the GTP-bound state of the GTPases (42,43). RTKN is an effector for RhoA-GTPase as it preferentially binds to RhoA-GTP (33). To gain insights into the predominant state of RhoA in the *Rpgr*$^{ko}$ retina, we performed a pull-down assay using recombinant glutathione S-transferase (GST)-tagged RTKN (GST-RTKN) and mouse retinal extracts loaded with non-hydrolyzable GTP analog (GTPγS). As shown in Figure 2E and F, we found a ~1.6-fold increase in the levels of RhoA pulled down by GST-RTKN in the GTPγS-loaded *Rpgr*$^{ko}$ retinal extracts when compared with the WT retinal extracts. No association between RhoA and purified GST protein was detected.

Actin cytoskeleton has been proposed to regulate basal disc orientation during OS morphogenesis (39). Ultrastructural analysis of the OS of the *Rpgr*$^{ko}$ mice revealed altered basal OS morphology even at 1 month of age, which progressed with age and was more prominent at 3 months of age (Supplementary Material, Fig. S1B).

### Expression of *Rpgr* in cone-dominant mouse retinas

Past work suggests that, in cases where the causative gene is expressed specifically in rods, secondary effects of rod loss manifest in cones as well. This is largely because rods account for the majority (97%) of photoreceptors in mammalian retina. However, in several instances, the causative gene (such as *RPGR*) is expressed in a variety of cell-types and mutations also manifest as early loss of cone function (44–46). Thus, it is conceivable that RPGR plays distinct roles in rods and cones and that cone death also involves the effect of the loss of RPGR directly on cone function. In primates, the fovea represents a cone-enriched region of the retina and dysfunction in this region results in the loss of daytime vision. To generate a cone-enriched model of RPGR loss, we utilized $Nrl^{-/-}$ mice, which develop cone-only retinas with a complete absence of rod photoreceptors. These mice express cone-specific genes and their cones display morphological and physiological features of WT cones (47,48). Thus, there is a great utility of $Nrl^{-/-}$ mice to understand cone biology and responses of human fovea during disease, as evident from previous studies to assess primary and secondary effects of retinal degeneration on cones (49–51).

We first performed qRT-PCR using RNA from retinas of WT (rod-dominant) and $Nrl^{-/-}$ mice. Compared with the WT mice, we found a ~2-fold up-regulation of *Rpgr* transcript expression in the $Nrl^{-/-}$ retina (Fig. 3A). Although our analysis of *Rpgr* expression in the WT mice is also taking into account its levels in cones, such levels would be minimal compared with 95–97% rod photoreceptors.

### Generation and characterization of *Rpgr*-DKO mice

We, next, generated *Rpgr*-DKO mice by breeding the $Rpgr^{ko}$ mice to the $Nrl^{-/-}$ mice. The loss of RPGR was validated by immunoblot analysis of mouse retinal extracts using a previously reported anti-RPGR antibody (21). As shown in Figure 3B, expression of both major isoforms of RPGR: constitutive RPGR ($RPGR^{const}$) and $RPGR^{ORF15}$ is undetectable in the *Rpgr*-DKO mice. We also tested whether the loss of RPGR results in alterations in the expression of other cone-specific genes. qRT-PCR and immunoblot analyses revealed no differences in the expression of S-cone opsin (Fig 3C and D) and cone alpha subunit of cone phosphodiesterase (data not shown) between *Rpgr*-DKO and $Nrl^{-/-}$ mouse retinas. The amount of protein loaded in the gel (20 µg) is such that S-opsin expression is undetectable in the WT mouse retina so that higher expression in $Nrl^{-/-}$ and *Rpgr*-DKO mouse retina is easily detected.

### Cone function alterations in *Rpgr*-DKO

Previous studies using animal models and *RPGR* patient information revealed a decline in both rod and cone function with age (15,52,53). Using the *Rpgr*-DKO mice, we conducted an age-dependent functional analysis of light signal processing in the absence of rods using ERG. As controls, we used age-matched $Nrl^{-/-}$ mice. Consistent with previous studies (47,48), $Nrl^{-/-}$ photopic ERG amplitude was relatively higher when compared with the WT mice (data not shown). Interestingly, we detected even higher (supranormal) photopic amplitude (~2-fold high) in the *Rpgr*-DKO mice (Fig. 4A). Analysis of Flicker ERG waveforms also showed similar results (Fig. 4B). There were sharp triangular waveforms in *Rpgr*-DKO mice at all ages tested as opposed to although sharp, but low-amplitude waveforms in $Nrl^{-/-}$ mice. Such sharp responses are typical of functional cone photoreceptors. Although there was progressive decline of cone response in *Rpgr*-DKO mice, the function was significantly higher even up to 9 months of age when compared with $Nrl^{-/-}$ mice. As expression levels of other cone proteins are similar in the two mouse models, such differences are unlikely to be due to differences in cone cell number.

Rosette formation is a hallmark of $Nrl^{-/-}$ mice (48,54) and has been reported to be associated with the loss of photoreceptor function (50,55,56). We, therefore, examined the effect of the loss of *Rpgr* on rosette formation by using retinal cross sections and whole mounts. As shown in Figure 4C and Supplementary Material, Figure S2, we observed mild decrease (~25%) in the number of rosettes in the *Rpgr*-DKO retina when compared with the $Nrl^{-/-}$ retina.

### Retinal morphology and protein trafficking in *Rpgr*-DKO mice

To assess the effect of the loss of RPGR on the morphology of the cone-only retina, we performed histological analysis of retinal sections at different stages. As shown in Figure 5A, the ONL (composed of photoreceptor nuclei) in the *Rpgr*-DKO mice was similar in thickness to that of the $Nrl^{-/-}$ retinas at 1 month of age. However, whereas $Nrl^{-/-}$ mice showed a decline in ONL thickness (consistent with previous reports of photoreceptor degeneration

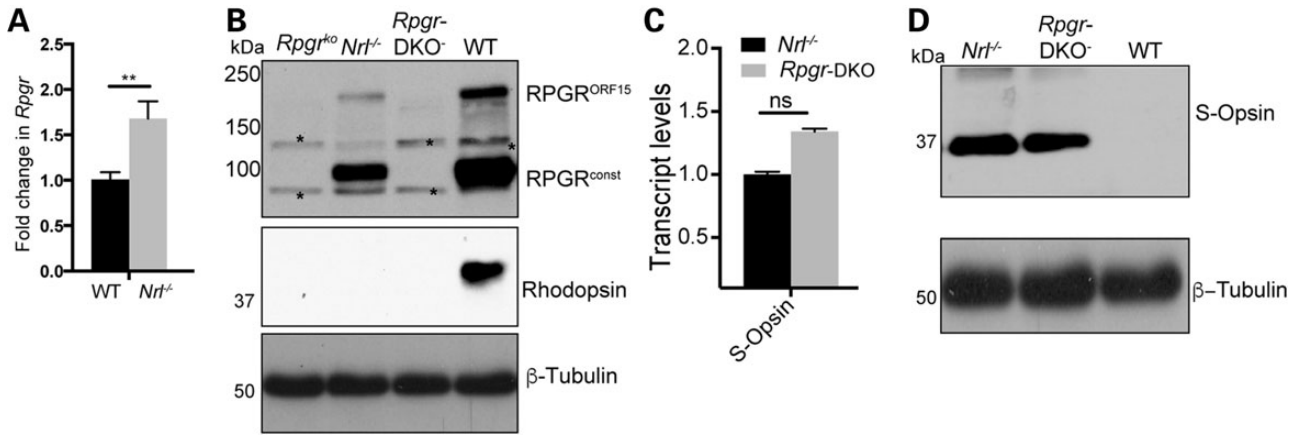


**Figure 3.** Characterization of *Rpgr*-DKO mice. (**A**) qRT-PCR analysis of WT and $Nrl^{-/-}$ mice was performed using primers that recognize all *Rpgr* isoforms (*Rpgr*), $^{**}P < 0.01$ (*t*-test). The data represent three biological replicates. (**B**) An equal amount of protein extracts (20 µg) of $Rpgr^{ko}$, $Nrl^{-/-}$, *Rpgr*-DKO and WT mice were analyzed by SDS–PAGE and immunoblotting using indicated antibodies. Asterisks represent non-specific immunoreactive signal. No change in transcript (**C**) or protein (**D**) levels of cone-specific S-opsin was detected in the *Rpgr*-DKO mice. Apparent molecular-weight markers are shown in kilodaltons (kDa). ns: not significant.

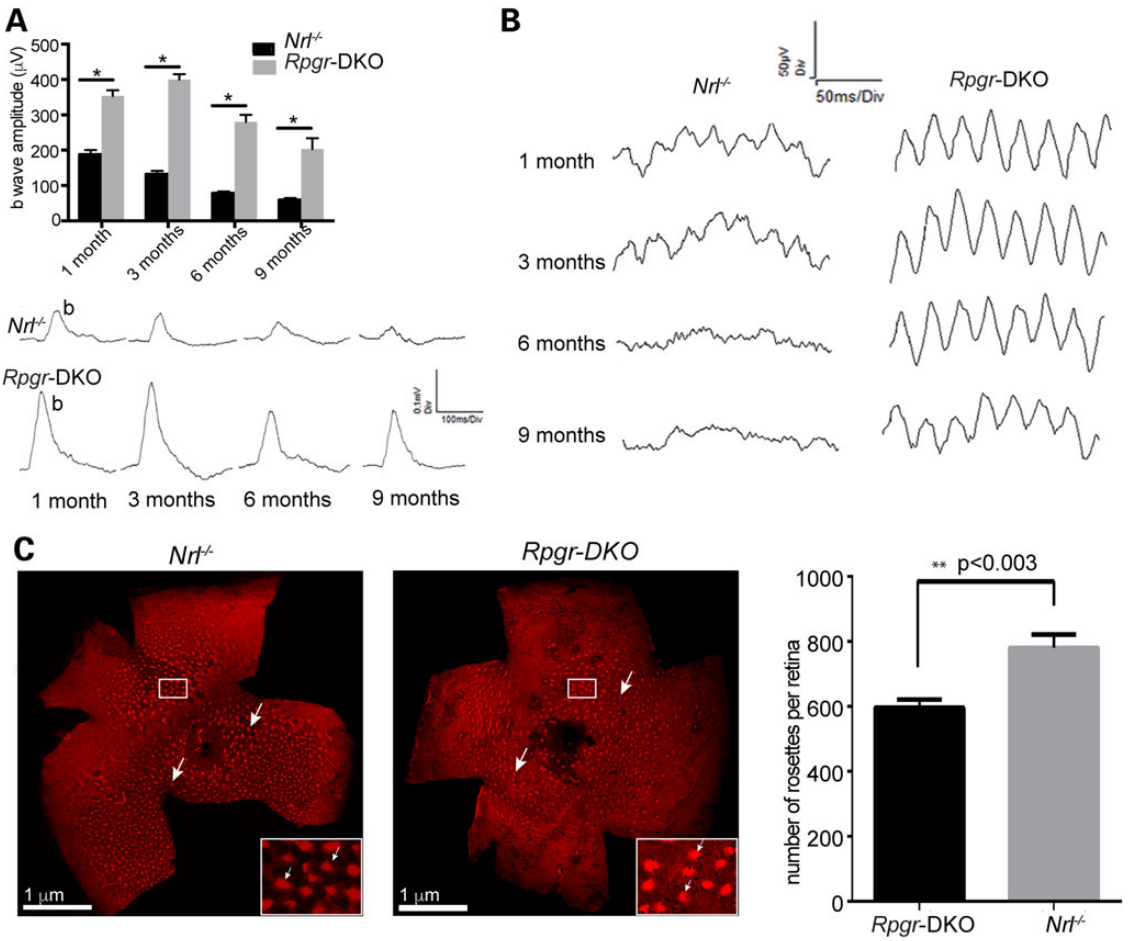


**Figure 4.** Phenotypic analysis of *Rpgr*-DKO mice. (**A**) Photopic b-wave response was analyzed by ERG at indicated ages of the $Nrl^{-/-}$ and the *Rpgr*-DKO mice. $P < 0.00001$. At least 10 mice of each genotype were tested in this experiment. Waveforms are represented in the lower panel. (**B**) Flicker (30 Hz) ERG waveforms of $Nrl^{-/-}$ and *Rpgr*-DKO mice showed distinct improvement in *Rpgr*-DKO mice with sharp triangular waveforms, which are typical of functional cone photoreceptors. (**C**) Whole mounts of retinas from $Nrl^{-/-}$ and *Rpgr*-DKO mice were stained with PNA (red). Arrows indicate rosettes. Inset shows higher magnification of the rosettes in the region enclosed in a rectangle. Quantitative analysis (right panel) revealed a significant reduction in the number of rosettes in the *Rpgr*-DKO mice (**$P < 0.003$).

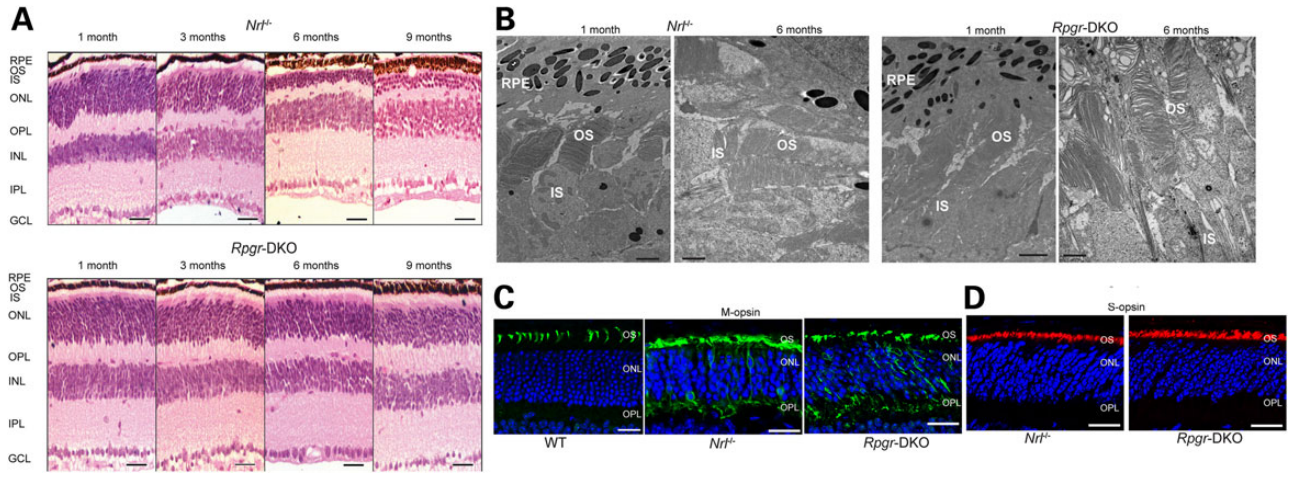


**Figure 5.** Retinal morphology and protein trafficking in *Rpgr*-DKO mice. (**A**) Histological analysis of $Nrl^{-/-}$ and *Rpgr*-DKO mice ($n = 10$) was performed at indicated ages. Although $Nrl^{-/-}$ mice showed progressive and faster deterioration of the thickness of ONL, considerably slow deterioration of the ONL was observed in *Rpgr*-DKO mice with relatively preserved thickness even up to 9 months of age. (**B**) TEM analysis of the $Nrl^{-/-}$ and *Rpgr*-DKO mice ($n = 3$) was performed at 1and 6 months of age. Although no difference was observed at 1 month, slightly altered OS architecture was detected in the *Rpgr*-DKO mice at 6 months of age. OS: outer segment; IS: inner segment; RPE: retinal pigment epithelium. Scale bar in 1-month-*Rpgr*-DKO image: 2 μm; scale bar in the rest of the images: 1 μm. (**C** and **D**) Retinal cryosections of 3-month-old WT, $Nrl^{-/-}$ and *Rpgr*-DKO mice (five each) were stained with indicated antibodies M-opsin (C; green) or S-opsin (D; red). Nuclei are stained with Hoechst (blue). OS: outer segment; ONL: outer nuclear layer; OPL: outer plexiform layer. Scale bar: 50 μm.

in these mice (54) at 3, 6 and 9 months of age, the *Rpgr*-DKO mouse retina showed relative delay in the decline in ONL thickness, with a thicker ONL even at 9 months of age. Ultrastructural analysis of mouse retinas at early age (1 month; prior to onset of degeneration in $Nrl^{-/-}$ retina) and later stage (6 months) corroborated our histological analysis. We found no apparent difference in cone morphology between the *Rpgr*-DKO and the $Nrl^{-/-}$ mice at 1 month of age whereas cone OS morphology was altered slightly at 6 months of age in *Rpgr*-DKO (Fig.5B). Overall, these data suggest that the loss of RPGR in mice spares cone development, but not maintenance.

RPGR is proposed to regulate ciliary protein trafficking in photoreceptors (22,26,57). To test whether *Rpgr*-DKO mice also exhibit protein trafficking defects, we performed immunofluorescence analysis using antibodies against cone outer segment (COS) proteins in *Rpgr*-DKO and $Nrl^{-/-}$ mouse retinas. Consistent with the previous observations using the $Rpgr^{ko}$ mice (27,28), we found mis-localization of M-opsin in the *Rpgr*-DKO mice (Fig. 5C). Although the $Nrl^{-/-}$ mice exhibit M-opsin mis-localization, this effect is more pronounced in the *Rpgr*-DKO mice. As control, no mis-localization was observed in the WT mouse retina. We did not observe any change in S-opsin trafficking in the *Rpgr*-DKO mice (Fig. 5D). This could either be because there is minor S-opsin mis-localization, which escaped our detection limits or because S-opsin mis-localizes secondary to rod degeneration in the $Rpgr^{ko}$ mice.

## Fatty acid analysis of the *Rpgr*-DKO retinas

Previous studies showed that build-up of polyunsaturated fatty acids, such as docosahexaenoic acid (DHA; C22:6n3) and very long-chain fatty acids results in supranormal ERG responses (58). DHA is the most abundant fatty acid in the phospholipids of rod OSs. It has been shown that abnormal build-up of DHA and other long-chain fatty acids leads to supranormal ERG responses in mice. We, therefore, hypothesized that the cone-enriched *Rpgr*-DKO retinas have altered fatty acid content, which results in a hyperabnormal ERG response. To test this hypothesis, we assessed the fatty acid composition of phospholipids in the *Rpgr*-DKO retinas and compared it to that in the $Nrl^{-/-}$ retinas. First, we observed that the major fatty acids in the cone-rich $Nrl^{-/-}$ retinas are: stearic acid (C18; ~28%), palmitic acid (C16; ~25%), DHA (C22:6n3; ~20%), oleic acid (C18:1; ~14%) and arachidonic acid (C20:4n6; ~10%) (Fig. 6A). As evident, DHA is not the most abundant fatty acid in the cone-rich retinas. Analysis of the *Rpgr*-DKO mice revealed that the level of DHA was significantly ($P < 0.05$) reduced when compared with the $Nrl^{-/-}$ mice. No significant change in other fatty acids was detected in this analysis.

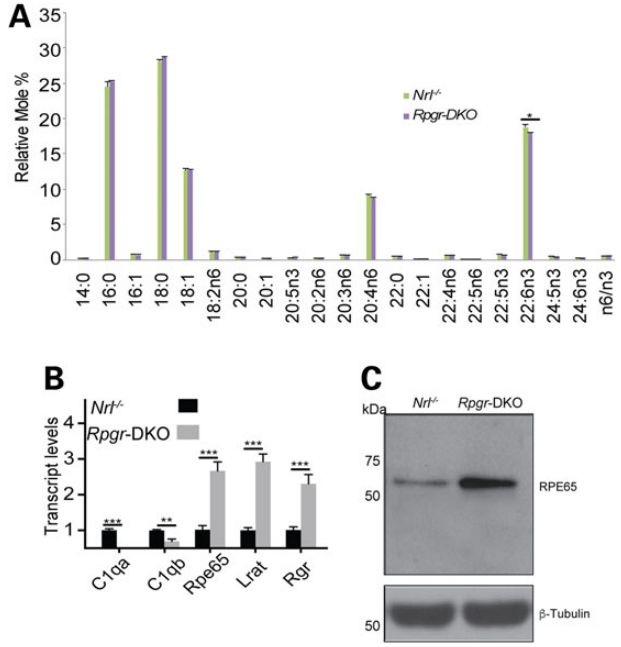


**Figure 6.** Alterations in the *Rpgr*-DKO retinas. (**A**) Fatty acid composition of the $Nrl^{-/-}$ and *Rpgr*-DKO mice retina was assessed, as described in the 'Materials and Methods' section. Data are mean ± SD for $n = 6$ samples. *$P < 0.05$. (**B**) qRT-PCR of the indicated genes was performed using retinal/RPE RNA from 1-month-old $Nrl^{-/-}$ or *Rpgr*-DKO mice. The results represent three biological replicates. (**C**) Immunoblot analysis using the anti-RPE65 antibody revealed increased protein levels in the *Rpgr*-DKO mice when compared with $Nrl^{-/-}$ mice. Anti-β-tubulin antibody was used as loading control.

## Transcriptomic analysis of *Rpgr*-DKO mice

Our data show that the loss of RPGR does not affect cone ultrastructure and protein trafficking, but there is a significant increase in the cone function. To gain insights into the pathways underlying such an effect, we assessed the transcriptome of the *Rpgr*-DKO mice when compared with the $Nrl^{-/-}$ mice. We compared the samples at 1 month of age when there is no apparent degeneration in the $Nrl^{-/-}$ and the *Rpgr*-DKO mice. We identified 110 differentially expressed genes based on a cut-off of at least 2-fold change in the expression level between the two groups (Supplementary Material, Table S4). IPA revealed that these genes belong to five major molecular functions: cell-to-cell signaling and interaction, cellular function and maintenance, cellular movement, cellular development and cellular growth and proliferation (Supplementary Material, Table S5). Of these, 12 genes were identified as parts of four canonical pathways that are altered in the diseased retina: visual cycle, complement system, retinol biosynthesis and phototransduction pathway (Supplementary Material, Table S6). The majority of these pathways including the complement system and visual cycle are implicated in Leber congenital amaurosis (LCA) and age-related macular degeneration (59,60). We, therefore, validated the alteration of two of the complement genes by qPCR and found a 2- to 3-fold down-regulation of *C1qa* and *C1qb*.

Among the up-regulated genes associated with visual cycle regulation, we detected a ~2.5-fold increase in *Rgr* (retinal G-protein-coupled receptor) and ~3-fold increase in *Lrat* (lecithin: retinol acyltransferase) (61–63) (Fig. 6B). We also observed a 3-fold increase in *Rpe65* (retinal pigment epithelium 65) (Fig. 6B), which is involved in chromophore recycling (64–66). Importantly, mutations in these three genes are associated with retinal degeneration (59,67,68). Immunoblot analysis of RPE extracts from the $Nrl^{-/-}$ and the *Rpgr*-DKO mice revealed ~2.5-fold increase in RPE65 protein levels (Fig. 6C; Supplementary Material, Fig. S3).

# Discussion

RPGR-XLRP is considered one of the most severe forms of RP and is associated with complex phenotypic presentation of differential rod or cone disease (11,12,69–71). With recent advances in gene therapy for RPGR-XLRP in the mouse and canine models (52,72) and the observation of rescue of *rpgr*-knock-down-associated phenotype in zebrafish studies (73), it is imperative to now design a suitable therapeutic plan for patients by

understanding rod and cone disease pathogenesis. Our studies have revealed different effects of the loss of RPGR on rod and cone-rich retinas and identified potential pathways that are altered during disease.

## Loss of RPGR in cone-rich retina

Our analysis of the *Rpgr*-DKO mice revealed new information on unusually preserved cone population and supranormal cone function. Other reports using the $Nrl^{-/-}$ retina have also revealed relatively slow cone loss due to mutations in genes expressed in both rods and cones, such as *Cep290*, *peripherin/Rds*, *Rpe65*, *Grk1* and insulin receptor (49–51,55,74–76). On the one hand, the *Rpgr*-DKO mice showed partial rescue of ONL degeneration of the $Nrl^{-/-}$ mice, while on the other hand, they exhibited even higher ERG responses. Although $Nrl^{-/-}$ mice exhibit higher cone ERGs when compared with WT mice, our results show that these ERGs can be even higher in the absence of RPGR. These observations indicate that the loss of RPGR potentially overcomes a negative effect on cone ERGs in the $Nrl^{-/-}$ mice and suggest a potential genetic interaction between NRL and RPGR. Since NRL is a transcription factor and some RPGR isoforms are also expressed in the nucleus (19), an association between these two proteins cannot be ruled out at this stage.

It has been reported that patients with macular degeneration or RP can present with supranormal photopic response (77). However, clinical testing for such ERG changes may not be feasible in all patients as they may present a late stage of the disease by which time the cone function has already deteriorated. Nonetheless, our results support the idea that patients or individuals with XLRP can be assessed for hyperabnormal cone response at their earliest clinic visit. It should be noted that the $Nrl^{-/-}$ mice developed increased number of S-cones, which form a minority population in human retina. Therefore, if the enhanced response were predominantly S-cone enriched, then a spatial testing using multifocal ERG or visual field test would be beneficial for early diagnosis of patients.

Several scenarios may account for the unusual cone response that we observed in the *Rpgr*-DKO mice. (i) An inherent property of the $Nrl^{-/-}$ retina: such a scenario seems unlikely because several previous studies have shown that ablation of a retinal disease gene in the $Nrl^{-/-}$ mice results in a decrease in the cone function and deterioration of retinal morphology (49–51). Therefore, we hypothesize that the effect that we have observed is specifically due to the loss of *Rpgr* on the $Nrl^{-/-}$ background. (ii) The $Nrl^{-/-}$ mouse retina develops rosettes, which can result in artifacts: it has been hypothesized that such structures are formed due to aberrant photoreceptor-Muller glia interactions, activity of RPE65 or photoreceptor-RPE interactions (50,55,56). However, those studies have not shown association between reductions in rosettes and increased cone function. Intriguingly, reduction in rosettes was shown in the $Rpe65^{ko}$ and *Rpe65* hypomorphic mutation on the $Nrl^{-/-}$ background (55,56). However, our studies show that reduction in rosettes is associated with increased levels of *Rpe65* and *Lrat*. We hypothesize that while the loss of *Rpe65* more significantly affects rosette formation, the loss of RPGR has a low-to-moderate effect on rosette formation, which is independent of its effect on the levels of *Rpe65* and *Lrat*. Therefore, it is also unlikely that the mild reduction in whorls and rosettes is contributing to the increased photopic amplitude of the *Rpgr*-DKO mice. (iii) A more likely scenario is that there is a predominant cone visual cycle dysfunction in the absence of RPGR. This is evident from the predominant alterations in the expression of RPE-specific genes in the *Rpgr*-DKO mice and alterations in the DHA levels of the *Rpgr*-DKO retinas. Changes in the fatty acid composition are predicted to affect the fluidity of the OS membranes and may result in altered ERGs. Previous studies showed that accumulation of DHA and other long-chain fatty acids is associated with supranormal ERG responses (58). However, the *Rpgr*-DKO mice showed a mild decrease in DHA levels when compared with the $Nrl^{-/-}$ mice. Additional investigations are necessary to delineate the significance and physiological relevance of reduced the DHA and function of cone-rich retinas.

Our studies suggest that either RPGR plays a critical role in the RPE or that up-regulation of the visual cycle-associated genes in the RPE is a secondary effect of altered light processing capacity of cones in the absence of RPGR. The light-sensitive chromophore 11-*cis* retinal is bound to the opsin and upon activation by light quanta, isomerizes to all-trans retinol. This initiates the phototransduction cascade (78). The all-trans retinol is then trafficked to the RPE where it is acted upon by LRAT to produce all-trans retinyl esters followed by action of RPE65 to produce 11-*cis* retinol. These cascades result in the recycling of the chromophore, which is then returned to the OS (51,56). It has been proposed that cones may possess distinct mechanisms of faster regeneration kinetics of the chromophore to better adapt to light conditions that allow uninterrupted daytime vision (79). An increase in *Rpe65*, *Lrat* as well as *Rgr* expression would enhance the rate of synthesis of reaction intermediates, which would increase the chromophore regeneration rate. Further studies are needed to test this hypothesis.

## Loss of RPGR in rod-dominant mice

We found predominant alterations in actin dynamics-associated pathways in our analyses of the $Rpgr^{ko}$ retina. The actin cytoskeleton is proposed to regulate basal OS disc alignment as well as photoreceptor axon retraction (34,39,80,81). Our analysis of RhoA activation and increased F- to G-actin ratio at 1 month of age indicate an early involvement of cytoskeletal defects in the $Rpgr^{ko}$ mice. In support of this hypothesis, we detected altered basal OS morphology in the $Rpgr^{ko}$ mice, prior to onset of photoreceptor dysfunction and degeneration. However, we did not detect significant alteration in ERG at early stages of the $Rpgr^{ko}$ mice. We reckon that these initial changes in actin dynamics may not significantly alter photoreceptor function at early stages whereas a slow and progressive build-up of the insult due to cytoskeletal alterations eventually lead to ciliary dysfunction and photoreceptor degeneration.

Although molecular mechanisms underlying the activation of RhoA in ciliary dysfunction are still unclear, it was shown that RhoA-GTP levels are also up-regulated in the absence of BBS-associated proteins (37). Thus, interplay between RPGR and BBS proteins to regulate actin cytoskeletal dynamics in the retina cannot be ruled out at this stage. Given an association of actin polymerization with cilia length control (38) and the involvement of RPGR and BBS proteins in the ciliary function, we propose that deregulation of actin cytoskeleton plays a significant role in the pathogenesis of retinal ciliopathies as well as syndromic ciliopathies.

Photoreceptor OS undergoes periodic disc shedding at the distal tips, which involves phagocytosis of the shed discs by the RPE (3). Actin cytoskeleton and specifically Myosin 7A is shown to play crucial roles in the phagocytosis of the shed discs and phagosomes and melanosome transport in the RPE. It would be interesting to examine RPE pathology in RPGR-associated disease.

Overall, our results show (i) an unexpected response of cone photoreceptors and (ii) involvement of distinct pathways associated with rod and cone dysfunction, due to the loss of *RPGR*. Additional investigations are necessary to evaluate the mechanisms underlying such defects. The deregulated pathways are also implicated in other retinal degenerative diseases, such as LCA, BBS, Usher syndrome and other syndromic ciliopathies. Therefore, our studies may provide crucial insights and identify potential commonalities among multiple retinal diseases that cause degeneration and dysfunction of photoreceptors.

## Materials and Methods

### Animals

All animal procedures and experiments were performed in accordance with the guidelines of Institutional Animal Care and Use Committee. Mice were housed in animal facility at University of Massachusetts Medical School, where they were maintained on a standard diet in a 12 h light to 12 h dark cycle. Lighting conditions were kept constant in all cages with illumination of 10–15 lux at the level of the cages. The $Nrl^{-/-}$ and $Rpgr^{ko}$ mice were procured from Dr Anand Swaroop and Dr Tiansen Li (National Eye Institute), respectively. Homozygous $Nrl^{-/-}$ and $Rpgr^{ko}$ mice were bred to generate *Rpgr*::$Nrl^{-/-}$ DKO mice. Genotypes were confirmed by PCR genotyping and immunoblotting analysis. All mice were also genotyped to exclude the *rd1* and *rd8* alleles.

### Primers and antibodies

List of antibodies and primers used in the present study is provided as Supplementary Material, Tables S7 and S8.

### ERG, histology and immunofluorescence

ERGs were recorded as described previously by using the Espion $e^2$ recording system (Diagnosys, Lowell, MA, USA) (82,83). For scotopic response, mice were dark-adapted overnight and all procedures were performed under dim red light. Light-adapted (Photopic) ERGs were recorded after light adaptation with a background illumination of 30 cd/$m^2$ (white 6500 K) for 8 min by two protocols: (i) the stimulus strength of 10 cd.s/$m^2$ was chosen for single flash. Twenty trials were averaged for single-flash responses and (ii) 30 Hz flicker ERG was performed under photopic conditions.

Histological and immunofluorescence analyses of paraffin- and cryopreserved retina and of flat mounts were performed as described (82–84). All images were taken by using a scanning confocal microscope (Leica TCS SP5 II laser; Leica Microsystems).

Transmission electron microscopy: eyes were collected from euthanized mice and fixed in 2.5% glutaraldehyde in 0.1 M sodium cacodylate buffer (pH 7.2) for 20 min at room temperature, as described (82). Specimens were visualized with a transmission electron microscope (Philips CM-10; Philips, Eindhoven, The Netherlands), coupled with a charge-coupled device digital camera (Gatan Erlangshen 785; Gatan, Inc., Warrendale, PA, USA).

### RNA sequencing

The total RNA was extracted from 1-month WT, $Rpgr^{ko}$, $Nrl^{-/-}$ and *Rpgr*-DKO mice by using RNeasy plus mini kit (Qiagen, USA) according to manufacturer's instructions. The starting sample was consisted of neuroretina + RPE (including choroid). Three biological replicates were included for each genotype. The quantity of RNA was measured by using spectrophotometer (Nanodrop, Thermo Scientific, USA) and quality of all samples was examined on the Agilent 2100 bio-analyzer using the RNA 6000 Nano Chip (Agilent Technologies, Santa Clara, CA, USA). We only included RNA samples with a RNA integrity number value >8. All subsequent steps were performed at Beijing Genomics Institute (Hong Kong). RNA samples were first treated with DNase I, followed by purification of poly (A) RNA using magnetic beads. To prepare libraries, mRNA was fragmented into short fragments, and the first-strand of cDNA was synthesized using random hexamer-primed reverse transcription. Buffers, dNTPs, RNase H and DNA polymerase I were added to synthesize the second-strand. The double-strand cDNA was purified using magnetic beads followed by end repair and Ion Proton adaptors were ligated to the ends of these fragments. Ligated products were selected by size and purified by using Tris-acetate-EDTA-agarose gel. Finally, the fragments were enriched using PCR amplification, purified using magnetic beads and dissolved in appropriate amount of Epstein–Barr solution. Quality of the sample library was determined by using Agilent 2100 Bioanalyzer and these products were sequenced via the Ion Proton platform according to the manufacturer's specifications. Data were collected and bioinformatics analysis was performed.

### Bioinformatics analysis

To estimate gene expression levels, we used RPKM (reads per kilobase per million mapped reads) values. To estimate differential expression of genes, we calculated $\log_2$ ratio from the RPKM values. To identify the genes with potential biological significance, we selected based on their $\log_2$ values either >1 or <−1, FDR of <0.05 and *P*-value < 0.05. We selected genes that were significantly altered at least 2-fold difference in all biological replicates. For pathway and network analyses, we used IPA (Ingenuity Systems, Redwood City, CA, USA; www.ingenuity.com) and DAVID software. The analysis was performed in two ways: (i) with all tissues and (ii) with retina only.

### Real-time qRT-PCR

Differentially expressed genes were chosen for further validation by qRT-PCR analysis. The total RNA from all the mice by using an RNeasy plus mini kit (Qiagen), with gDNA eliminator columns to remove any contaminating genomic DNA. Primers were designed to amplify fragments of 120–200 bp, with shorter fragments preferred. Approximately 1 µg of total RNA was reverse transcribed to cDNA by using a Verso™ cDNA Kit (Thermo Fisher Scientific) and qPCR was performed on Bio-Rad CFX96 Real-time PCR Detection System (Bio-Rad) by using SsoFast EvaGreen Supermix (Bio-Rad). Reactions were performed in duplicates for at least three biological replicates. The *Ct* values were normalized to a loading control (glyceraldehyde 3-phosphate dehydrogenase (GAPDH) and β-tubulin). Gene-expression fold changes were calculated using the ΔΔCT method where the relative expression is calculated as $2^{-\Delta\Delta Ct}$ and *Ct* represents the threshold cycle. The data are presented based on the published guidelines (85). Fold change was calculated considering relative gene expression of control sample as '1'.

### F-/G-actin measurements

Retinal fractionation to obtain the F- and G-actin fractions was performed as described (37,86,87). Briefly, fresh retinas from WT and $Rpgr^{ko}$ (six retinas from each genotype) were homogenized

in F-actin stabilization buffer (50 mM piperazine-N,N′-bis(2-ethanesulfonic acid at pH 6.9, 50 mM NaCl, 5 mM $MgCl_2$, 5 mM ethylene glycol tetraacetic acid, 5% glycerol, 0.1% NP40, 0.1% Triton X-100, 0.1% Tween 20, 0.1% β-mercaptoethanol, 1 mM adenosine triphosphate, protease inhibitor cocktail) and passed several times through a 29-G syringe. The lysate was incubated at 37°C for 10 min and then centrifuged at 350 × *g* for 5 min to remove cell debris. Supernatant was collected and centrifuged again at 100 000 × *g* for 1 h. The resultant supernatant was transferred immediately into another tube and was used as the G-actin fraction. The pellet was resuspended in equal volume of the buffer containing 100 µM cytochalsin D and kept on ice for 60 min with gentle mixing for every 15 min. Samples were then sonicated and centrifuged and the supernatant was collected for F-actin fraction. The G- and F-actin fractions were analyzed by immunoblotting. Fold change was calculated considering relative band intensity of control sample as '1'.

### RhoA activation assay

RhoA activity assay was performed with the use of a Rho activation assay kit (Cytoskeleton) in accordance with the manufacturer's instructions. Briefly, fresh retinas (six retinas each genotype) were dissected and were lysed in ice-cold lysis buffer. The resultant homogenate was centrifuged at 1700 × *g* for 10 min at 4°C. Supernatant was collected into fresh tube and 20 µg of GST or GST-RTKN conjugated beads were added in the presence of GTPγS. These samples were incubated on a nutator for 1 h at 4°C. Samples were then centrifuged at 4000 rpm and the beads were washed three times with wash solution. Final bead pellet was resuspended in sample buffer, boiled for 5 min and analyzed by sodium dodecyl sulfate–polyacrylamide gel electrophoresis (SDS–PAGE) and immunoblotting. Fold change was calculated considering relative band intensity of control sample as '1'.

### Lipid analysis

Fatty acid profiles were determined for retina. Total lipids were extracted following the method of Bligh and Dyer (88) with modifications (89). To each lipid extract were added 15:0 and 17:0 as internal standards. The lipid extracts were subjected to acid hydrolysis/methanolysis to generate fatty acid methyl esters (FAMEs) (90). FAMEs were quantified using an Agilent Technologies 6890N gas chromatograph with flame ionization detector (GC) (91). The results were also confirmed by GC-MS.

### Statistical analysis

All data are presented as means ± SEM. Data groups were compared by non-parametric *t*-tests (two groups) or multiple *t*-tests (more than two groups) using the GraphPad software. Differences between groups were considered statistically significant if $P < 0.05$. The statistical significance is denoted with asterisks (*$P$ = 0.01–0.05; **$P$ = 0.001–0.01; ***$P$ = 0.0001–0.001 and ****$P \leq 0.00001$).

## Supplementary Material

Supplementary Material is available at *HMG* online.

## Acknowledgements

We thank Dr John Heckenlively and Dr Visvanathan Ramamurthy for critical discussions about the data.

*Conflict of Interest statement*. None declared.

## Funding

This work is supported by grants from National Eye Institute (EY022372); University of Massachusetts Center for Clinical and Translational Sciences (UMCCTS); Foundation Fighting Blindness; Massachusetts Lions Eye Research Foundation (MLERF) and University of Massachusetts Cell Biology Confocal Core and Electron Microscopy Core (award no. S10RR027897).

## References

1. Kandel, E.R. (2013) *Principles of Neural Science*. McGraw-Hill, New York.
2. Besharse, J.C., Baker, S.A., Luby-Phelps, K. and Pazour, G.J. (2003) Photoreceptor intersegmental transport and retinal degeneration: a conserved pathway common to motile and sensory cilia. *Adv. Exp. Med. Biol.*, **533**, 157–164.
3. Williams, D.S. (2002) Transport to the photoreceptor outer segment by myosin VIIa and kinesin II. *Vision Res.*, **42**, 455–462.
4. Lamb, T.D. (2013) Evolution of phototransduction, vertebrate photoreceptors and retina. *Prog. Retin. Eye. Res.*, **36**, 52–119.
5. Insinna, C. and Besharse, J.C. (2008) Intraflagellar transport and the sensory outer segment of vertebrate photoreceptors. *Dev. Dyn.*, **237**, 1982–1992.
6. Dowling, J.E. (2012) *The Retina : an Approachable Part of the Brain*. Belknap Press of Harvard University Press, Cambridge, Mass.
7. Ferrari, S., Di Iorio, E., Barbaro, V., Ponzin, D., Sorrentino, F.S. and Parmeggiani, F. (2011) Retinitis pigmentosa: genes and disease mechanisms. *Curr. Genomics*, **12**, 238–249.
8. Bird, A.C. (1987) Clinical investigation of retinitis pigmentosa. *Prog. Clin. Biol. Res.*, **247**, 3–20.
9. Heckenlively, J.R., Yoser, S.L., Friedman, L.H. and Oversier, J.J. (1988) Clinical findings and common symptoms in retinitis pigmentosa. *Am. J. Ophthalmol.*, **105**, 504–511.
10. Daiger, S.P., Bowne, S.J. and Sullivan, L.S. (2007) Perspective on genes and mutations causing retinitis pigmentosa. *Arch. Ophthalmol.*, **125**, 151–158.
11. Fishman, G.A., Farber, M.D. and Derlacki, D.J. (1988) X-linked retinitis pigmentosa. Profile of clinical findings. *Arch. Ophthalmol.*, **106**, 369–375.
12. Churchill, J.D., Bowne, S.J., Sullivan, L.S., Lewis, R.A., Wheaton, D.K., Birch, D.G., Branham, K.E., Heckenlively, J.R. and Daiger, S.P. (2013) Mutations in the X-linked retinitis pigmentosa genes RPGR and RP2 found in 8.5% of families with a provisional diagnosis of autosomal dominant retinitis pigmentosa. *Invest. Ophthalmol. Vis. Sci.*, **54**, 1411–1416.
13. Meindl, A., Dry, K., Herrmann, K., Manson, F., Ciccodicola, A., Edgar, A., Carvalho, M.R., Achatz, H., Hellebrand, H., Lennon, A. *et al.* (1996) A gene (RPGR) with homology to the RCC1 guanine nucleotide exchange factor is mutated in X-linked retinitis pigmentosa (RP3). *Nat. Genet.*, **13**, 35–42.
14. Andreasson, S., Ponjavic, V., Abrahamson, M., Ehinger, B., Wu, W., Fujita, R., Buraczynska, M. and Swaroop, A. (1997) Phenotypes in three Swedish families with X-linked retinitis pigmentosa caused by different mutations in the RPGR gene. *Am. J. Ophthalmol.*, **124**, 95–102.
15. Jacobson, S.G., Buraczynska, M., Milam, A.H., Chen, C., Jarvalainen, M., Fujita, R., Wu, W., Huang, Y., Cideciyan, A.V. and Swaroop, A. (1997) Disease expression in X-linked retinitis pigmentosa caused by a putative null mutation in the RPGR gene. *Invest. Ophthalmol. Vis. Sci.*, **38**, 1983–1997.
16. Weleber, R.G., Butler, N.S., Murphey, W.H., Sheffield, V.C. and Stone, E.M. (1997) X-linked retinitis pigmentosa associated

with a 2-base pair insertion in codon 99 of the RP3 gene RPGR. *Arch. Ophthalmol.*, **115**, 1429–1435.
17. Ayyagari, R., Demirci, F.Y., Liu, J., Bingham, E.L., Stringham, H., Kakuk, L.E., Boehnke, M., Gorin, M.B., Richards, J.E. and Sieving, P.A. (2002) X-linked recessive atrophic macular degeneration from RPGR mutation. *Genomics*, **80**, 166–171.
18. Demirci, F.Y., Rigatti, B.W., Wen, G., Radak, A.L., Mah, T.S., Baic, C.L., Traboulsi, E.I., Alitalo, T., Ramser, J. and Gorin, M. B. (2002) X-linked cone-rod dystrophy (locus COD1): identification of mutations in RPGR exon ORF15. *Am. J. Hum. Genet.*,**70**, 1049–1053.
19. He, S., Parapuram, S.K., Hurd, T.W., Behnam, B., Margolis, B., Swaroop, A. and Khanna, H. (2008) Retinitis PigmentosaGTPase Regulator (RPGR) protein isoforms in mammalian retina: insights into X-linked Retinitis Pigmentosa and associated ciliopathies. *Vision Res.*, **48**, 366–376.
20. Hong, D.H. and Li, T. (2002) Complex expression pattern of RPGR reveals a role for purine-rich exonic splicing enhancers. *Invest. Ophthalmol. Vis. Sci.*, **43**, 3373–3382.
21. Hong, D.H., Pawlyk, B., Sokolov, M., Strissel, K.J., Yang, J., Tulloch, B., Wright, A.F., Arshavsky, V.Y. and Li, T. (2003) RPGR isoforms in photoreceptor connecting cilia and the transitional zone of motile cilia. *Invest. Ophthalmol. Vis. Sci.*, **44**, 2413–2421.
22. Khanna, H., Hurd, T.W., Lillo, C., Shu, X., Parapuram, S.K., He, S., Akimoto, M., Wright, A.F., Margolis, B., Williams, D.S. *et al.* (2005) RPGR-ORF15, which is mutated in retinitis pigmentosa, associates with SMC1, SMC3, and microtubule transport proteins. *J. Biol. Chem.*, **280**, 33580–33587.
23. Kirschner, R., Rosenberg, T., Schultz-Heienbrok, R., Lenzner, S., Feil, S., Roepman, R., Cremers, F.P., Ropers, H.H. and Berger, W. (1999) RPGR transcription studies in mouse and human tissues reveal a retina-specific isoform that is disrupted in a patient with X-linked retinitis pigmentosa. *Hum. Mol. Genet.*, **8**, 1571–1578.
24. Vervoort, R., Lennon, A., Bird, A.C., Tulloch, B., Axton, R., Miano, M.G., Meindl, A., Meitinger, T., Ciccodicola, A. and Wright, A.F. (2000) Mutational hot spot within a new RPGR exon in X-linked retinitis pigmentosa.*Nat. Genet.*, **25**, 462–466.
25. Anand, M. and Khanna, H. (2012) Ciliary transition zone (TZ) proteins RPGR and CEP290: role in photoreceptor cilia and degenerative diseases. *Expert Opin. Ther. Targets*, **16**, 541–551.
26. Rao, K.N., Li, L., Anand, M. and Khanna, H. (2015) Ablation of retinal ciliopathy protein RPGR results in altered photoreceptor ciliary composition. *Sci. Rep.*, **5**, 11137.
27. Hong, D.H., Pawlyk, B.S., Shang, J., Sandberg, M.A., Berson, E.L. and Li, T. (2000) A retinitis pigmentosaGTPase regulator (RPGR)-deficient mouse model for X-linked retinitis pigmentosa (RP3). *Proc. Natl Acad. Sci. USA*, **97**, 3649–3654.
28. Thompson, D.A., Khan, N.W., Othman, M.I., Chang, B., Jia, L., Grahek, G., Wu, Z., Hiriyanna, S., Nellissery, J., Li, T. *et al.* (2012) Rd9 is a naturally occurring mouse model of a common form of retinitis pigmentosa caused by mutations in RPGR-ORF15. *PLoS One*, **7**, e35865.
29. Zhang, Q., Acland, G.M., Wu, W.X., Johnson, J.L., Pearce-Kelling, S., Tulloch, B., Vervoort, R., Wright, A.F. and Aguirre, G.D. (2002) Different RPGR exon ORF15 mutations in Canids provide insights into photoreceptor cell degeneration. *Hum. Mol. Genet.*, **11**, 993–1003.
30. Brunner, S., Skosyrski, S., Kirschner-Schwabe, R., Knobeloch, K.P., Neidhardt, J., Feil, S., Glaus, E., Luhmann, U.F., Ruther, K. and Berger, W. (2010) Cone versus rod disease in a mutant Rpgr mouse caused by different genetic backgrounds. *Invest. Ophthalmol. Vis. Sci.*, **51**, 1106–1115.
31. Gakovic, M., Shu, X., Kasioulis, I., Carpanini, S., Moraga, I. and Wright, A.F. (2011) The role of RPGR in cilia formation and actin stability. *Hum. Mol. Genet.*, **20**, 4840–4850.
32. Khalil, B.D., Hanna, S., Saykali, B.A., El-Sitt, S., Nasrallah, A., Marston, D., El-Sabban, M., Hahn, K.M., Symons, M. and El-Sibai, M. (2014) The regulation of RhoA at focal adhesions by StarD13 is important for astrocytoma cell motility. *Exp. Cell Res.*, **321**, 109–122.
33. Collier, F.M., Gregorio-King, C.C., Gough, T.J., Talbot, C.D., Walder, K. and Kirkland, M.A. (2004) Identification and characterization of a lymphocytic Rho-GTPase effector: rhotekin-2. *Biochem. Biophys. Res. Commun.*, **324**, 1360–1369.
34. Fontainhas, A.M. and Townes-Anderson, E. (2011) RhoA inactivation prevents photoreceptor axon retraction in an in vitro model of acute retinal detachment. *Invest. Ophthalmol. Vis. Sci.*, **52**, 579–587.
35. Meindl, A., Carvalho, M.R., Herrmann, K., Lorenz, B., Achatz, H., Lorenz, B., Apfelstedt-Sylla, E., Wittwer, B., Ross, M. and Meitinger, T. (1995) A gene (SRPX) encoding a sushi-repeat-containing protein is deleted in patients with X-linked retinitis pigmentosa. *Hum. Mol. Genet.*, **4**, 2339–2346.
36. Burnicka-Turek, O., Kata, A., Buyandelger, B., Ebermann, L., Kramann, N., Burfeind, P., Hoyer-Fender, S., Engel, W. and Adham, I.M. (2010) Pelota interacts with HAX1, EIF3G and SRPX and the resulting protein complexes are associated with the actin cytoskeleton. *BMC Cell. Biol.*, **11**, 28.
37. Hernandez-Hernandez, V., Pravincumar, P., Diaz-Font, A., May-Simera, H., Jenkins, D., Knight, M. and Beales, P.L. (2013) Bardet-Biedl syndrome proteins control the cilia length through regulation of actin polymerization. *Hum. Mol. Genet.*, **22**, 3858–3868.
38. Kim, J., Lee, J.E., Heynen-Genel, S., Suyama, E., Ono, K., Lee, K., Ideker, T., Aza-Blanc, P. and Gleeson, J.G. (2010) Functional genomic screen for modulators of ciliogenesis and cilium length. *Nature*, **464**, 1048–1051.
39. Chaitin, M.H. and Burnside, B. (1989) Actin filament polarity at the site of rod outer segment disk morphogenesis. *Invest. Ophthalmol. Vis. Sci.*, **30**, 2461–2469.
40. Amano, M., Chihara, K., Kimura, K., Fukata, Y., Nakamura, N., Matsuura, Y. and Kaibuchi, K. (1997) Formation of actin stress fibers and focal adhesions enhanced by Rho-kinase. *Science*, **275**, 1308–1311.
41. Ridley, A.J. (2006) Rho GTPases and actin dynamics in membrane protrusions and vesicle trafficking. *Trends. Cell Biol.*, **16**, 522–529.
42. Rao, K.N. and Khanna, H. (2015) Role of small GTPases in polarized vesicle transport to primary cilium. *Res. Rep. Biol.*, **6**, 17–24.
43. Yoshimura, S., Haas, A.K. and Barr, F.A. (2008) Analysis of RabGTPase and GTPase-activating protein function at primary cilia. *Methods Enzymol.*,**439**, 353–364.
44. Leveillard, T., Mohand-Said, S., Lorentz, O., Hicks, D., Fintz, A. C., Clerin, E., Simonutti, M., Forster, V., Cavusoglu, N., Chalmel, F. *et al.* (2004) Identification and characterization of rod-derived cone viability factor. *Nat. Genet.*, **36**, 755–759.
45. Punzo, C., Kornacker, K. and Cepko, C.L. (2009) Stimulation of the insulin/mTOR pathway delays cone death in a mouse model of retinitis pigmentosa. *Nat. Neurosci.*, **12**, 44–52.
46. Wright, A.F., Chakarova, C.F., Abd El-Aziz, M.M. and Bhattacharya, S.S. (2010) Photoreceptor degeneration: genetic and mechanistic dissection of a complex trait. *Nat. Rev. Genet.*, **11**, 273–284.

47. Daniele, L.L., Lillo, C., Lyubarsky, A.L., Nikonov, S.S., Philp, N., Mears, A.J., Swaroop, A., Williams, D.S. and Pugh, E.N. Jr. (2005) Cone-like morphological, molecular, and electrophysiological features of the photoreceptors of the Nrl knockout mouse. *Invest. Ophthalmol. Vis. Sci.*, **46**, 2156–2167.
48. Mears, A.J., Kondo, M., Swain, P.K., Takada, Y., Bush, R.A., Saunders, T.L., Sieving, P.A. and Swaroop, A. (2001) Nrl is required for rod photoreceptor development. *Nat. Genet.*, **29**, 447–452.
49. Cideciyan, A.V., Rachel, R.A., Aleman, T.S., Swider, M., Schwartz, S.B., Sumaroka, A., Roman, A.J., Stone, E.M., Jacobson, S.G. and Swaroop, A. (2011) Cone photoreceptors are the main targets for gene therapy of NPHP5 (IQCB1) or NPHP6 (CEP290) blindness: generation of an all-cone Nphp6 hypomorph mouse that mimics the human retinal ciliopathy. *Hum. Mol. Genet.*, **20**, 1411–1423.
50. Farjo, R., Fliesler, S.J. and Naash, M.I. (2007) Effect of Rds abundance on cone outer segment morphogenesis, photoreceptor gene expression, and outer limiting membrane integrity. *J. Comp. Neurol.*, **504**, 619–630.
51. Feathers, K.L., Lyubarsky, A.L., Khan, N.W., Teofilo, K., Swaroop, A., Williams, D.S., Pugh, E.N. Jr. and Thompson, D.A. (2008) Nrl-knockout mice deficient in Rpe65 fail to synthesize 11-cis retinal and cone outer segments. *Invest. Ophthalmol. Vis Sci.*, **49**, 1126–1135.
52. Beltran, W.A., Cideciyan, A.V., Lewin, A.S., Iwabe, S., Khanna, H., Sumaroka, A., Chiodo, V.A., Fajardo, D.S., Roman, A.J., Deng, W.T. *et al.* (2012) Gene therapy rescues photoreceptor blindness in dogs and paves the way for treating human X-linked retinitis pigmentosa. *Proc. Natl Acad. Sci. USA*, **109**, 2132–2137.
53. Sharon, D., Sandberg, M.A., Rabe, V.W., Stillberger, M., Dryja, T.P. and Berson, E.L. (2003) RP2 and RPGR mutations and clinical correlations in patients with X-linked retinitis pigmentosa. *Am. J. Hum. Genet.*,**73**, 1131–1146.
54. Roger, J.E., Ranganath, K., Zhao, L., Cojocaru, R.I., Brooks, M., Gotoh, N., Veleri, S., Hiriyanna, A., Rachel, R.A., Campos, M.M. *et al.* (2012) Preservation of cone photoreceptors after a rapid yet transient degeneration and remodeling in cone-only Nrl-/- mouse retina. *J. Neurosci.*, **32**, 528–541.
55. Samardzija, M. and Grimm, C. (2014) Mouse models for cone degeneration. *Adv. Exp. Med. Biol.*, **801**, 567–573.
56. Samardzija, M., Caprara, C., Heynen, S.R., Willcox DeParis, S., Meneau, I., Traber, G., Agca, C., von Lintig, J. and Grimm, C. (2014) A mouse model for studying cone photoreceptor pathologies. *Invest. Ophthalmol. Vis. Sci.*, **55**, 5304–5313.
57. Murga-Zamalloa, C.A., Atkins, S.J., Peranen, J., Swaroop, A. and Khanna, H. (2010) Interaction of retinitis pigmentosaGTPase regulator (RPGR) with RAB8A GTPase: implications for cilia dysfunction and photoreceptor degeneration. *Hum. Mol. Genet.*, **19**, 3591–3598.
58. Suh, M., Sauve, Y., Merrells, K.J., Kang, J.X. and Ma, D.W. (2009) Supranormal electroretinogram in fat-1 mice with retinas enriched in docosahexaenoic acid and n-3 very long chain fatty acids (C24-C36). *Invest. Ophthalmol. Vis. Sci.*, **50**, 4394–4401.
59. den Hollander, A.I., Roepman, R., Koenekoop, R.K. and Cremers, F.P. (2008) Leber congenital amaurosis: genes, proteins and disease mechanisms. *Prog. Retin. Eye Res.*, **27**, 391–419.
60. Mullins, R.F., Faidley, E.A., Daggett, H.T., Jomary, C., Lotery, A. J. and Stone, E.M. (2009) Localization of complement 1 inhibitor (C1INH/SERPING1) in human eyes with age-related macular degeneration. *Exp. Eye Res.*, **89**, 767–773.
61. Ruiz, A., Winston, A., Lim, Y.H., Gilbert, B.A., Rando, R.R. and Bok, D. (1999) Molecular and biochemical characterization of lecithin retinol acyltransferase. *J. Biol. Chem.*, **274**, 3834–3841.
62. Maeda, T., Van Hooser, J.P., Driessen, C.A., Filipek, S., Janssen, J.J. and Palczewski, K. (2003) Evaluation of the role of the retinal G protein-coupled receptor (RGR) in the vertebrate retina in vivo. *J. Neurochem.*, **85**, 944–956.
63. Wenzel, A., Oberhauser, V., Pugh, E.N. Jr., Lamb, T.D., Grimm, C., Samardzija, M., Fahl, E., Seeliger, M.W., Reme, C.E. and von Lintig, J. (2005) The retinal G protein-coupled receptor (RGR) enhances isomerohydrolase activity independent of light. *J. Biol. Chem.*, **280**, 29874–29884.
64. Moiseyev, G., Chen, Y., Takahashi, Y., Wu, B.X. and Ma, J.X. (2005) RPE65 is the isomerohydrolase in the retinoid visual cycle. *Proc. Natl Acad. Sci. USA*, **102**, 12413–12418.
65. Redmond, T.M., Yu, S., Lee, E., Bok, D., Hamasaki, D., Chen, N., Goletz, P., Ma, J.X., Crouch, R.K. and Pfeifer, K. (1998) Rpe65 is necessary for production of 11-cis-vitamin A in the retinal visual cycle. *Nat. Genet.*, **20**, 344–351.
66. Seeliger, M.W., Grimm, C., Stahlberg, F., Friedburg, C., Jaissle, G., Zrenner, E., Guo, H., Reme, C.E., Humphries, P., Hofmann, F. *et al.* (2001) New views on RPE65 deficiency: the rod system is the source of vision in a mouse model of Leber congenital amaurosis. *Nat. Genet.*, **29**, 70–74.
67. Chen, P., Hao, W., Rife, L., Wang, X.P., Shen, D., Chen, J., Ogden, T., Van Boemel, G.B., Wu, L., Yang, M. *et al.* (2001) A photic visual cycle of rhodopsin regeneration is dependent on Rgr. *Nat. Genet.*, **28**, 256–260.
68. Morimura, H., Saindelle-Ribeaudeau, F., Berson, E.L. and Dryja, T.P. (1999) Mutations in RGR, encoding a light-sensitive opsin homologue, in patients with retinitis pigmentosa. *Nat. Genet.*, **23**, 393–394.
69. Fahim, A.T., Bowne, S.J., Sullivan, L.S., Webb, K.D., Williams, J. T., Wheaton, D.K., Birch, D.G. and Daiger, S.P. (2011) Allelic heterogeneity and genetic modifier loci contribute to clinical variation in males with X-linked retinitis pigmentosa due to RPGR mutations. *PLoS One*, **6**, e23021.
70. Sandberg, M.A., Rosner, B, Weigel-Difranco, C, Dryja,, T.P. and EL.,, B. (2007) Disease Course of Patients with X-linked Retinitis Pigmentosa due to RPGR Gene Mutations. *Invest. Ophthalmol. Vis. Sci.*, **48**, 1298–1304.
71. Zahid, S., Khan, N., Branham, K., Othman, M., Karoukis, A.J., Sharma, N., Moncrief, A., Mahmood, M.N., Sieving, P.A., Swaroop, A. *et al.* (2013) Phenotypic conservation in patients with X-linked retinitis pigmentosa caused by RPGR mutations. *JAMA Ophthalmol.*,**131**, 1016–1025.
72. Wu, Z., Hiriyanna, S., Qian, H., Mookherjee, S., Campos, M.M., Gao, C., Fariss, R., Sieving, P.A., Li, T., Colosi, P. *et al.* (2015) A long-term efficacy study of gene replacement therapy for RPGR-associated retinal degeneration. *Hum. Mol. Genet.*, **24**, 3956–3970.
73. Ghosh, A.K., Murga-Zamalloa, C.A., Chan, L., Hitchcock, P.F., Swaroop, A. and Khanna, H. (2010) Human retinopathy-associated ciliary protein retinitis pigmentosaGTPase regulator mediates cilia-dependent vertebrate development. *Hum. Mol. Genet.*, **19**, 90–98.
74. Zhu, X., Brown, B., Li, A., Mears, A.J., Swaroop, A. and Craft, C. M. (2003) GRK1-dependent phosphorylation of S and M opsins and their binding to cone arrestin during cone phototransduction in the mouse retina. *J. Neurosci.*, **23**, 6152–6160.
75. Farjo, R., Skaggs, J.S., Nagel, B.A., Quiambao, A.B., Nash, Z.A., Fliesler, S.J. and Naash, M.I. (2006) Retention of function without normal disc morphogenesis occurs in cone but not rod photoreceptors. *J. Cell. Biol.*, **173**, 59–68.

76. Rajala, A., Dighe, R., Agbaga, M.P., Anderson, R.E. and Rajala, R.V. (2013) Insulin receptor signaling in cones. *J. Biol. Chem.*, **288**, 19503–19515.
77. Heckenlively, J.R., Tanji, T. and Logani, S. (1994) Retrospective study of hyperabnormal (supranormal) electroretinographic responses in 104 patients. *Trans. Am. Ophthalmol. Soc.*, **92**, 217–231; discussion 231–213.
78. McBee, J.K., Palczewski, K., Baehr, W. and Pepperberg, D.R. (2001) Confronting complexity: the interlink of phototransduction and retinoid metabolism in the vertebrate retina. *Prog. Retin. Eye Res.*, **20**, 469–529.
79. Wang, J.S. and Kefalov, V.J. (2011) The cone-specific visual cycle. *Prog. Retin. Eye Res.*, **30**, 115–128.
80. Chaitin, M.H. (1992) Double immunogold localization of opsin and actin in the cilium of developing mouse photoreceptors. *Exp. Eye Res.*, **54**, 261–267.
81. Gilliam, J.C., Chang, J.T., Sandoval, I.M., Zhang, Y., Li, T., Pittler, S.J., Chiu, W. and Wensel, T.G. (2012) Three-dimensional architecture of the rod sensory cilium and its disruption in retinal neurodegeneration. *Cell*, **151**, 1029–1041.
82. Li, L., Khan, N., Hurd, T., Ghosh, A.K., Cheng, C., Molday, R., Heckenlively, J.R., Swaroop, A. and Khanna, H. (2013) Ablation of the X-linked retinitis pigmentosa 2 (Rp2) gene in mice results in opsinmislocalization and photoreceptor degeneration. *Invest. Ophthalmol. Vis. Sci.*, **54**, 4503–4511.
83. Li, L., Anand, M., Rao, K.N. and Khanna, H. (2015) Cilia in photoreceptors. *Methods Cell Biol.*, **127**, 75–92.
84. Subramanian, B., Anand, M., Khan, N.W. and Khanna, H. (2014) Loss of Raf-1 kinase inhibitory protein delays early-onset severe retinal ciliopathy in Cep290rd16 mouse. *Invest. Ophthalmol. Vis. Sci.*, **55**, 5788–5794.
85. Bustin, S.A., Benes, V., Garson, J.A., Hellemans, J., Huggett, J., Kubista, M., Mueller, R., Nolan, T., Pfaffl, M.W., Shipley, G.L. *et al.* (2009) The MIQE guidelines: minimum information for publication of quantitative real-time PCR experiments. *Clin. Chem.*, **55**, 611–622.
86. Albinsson, S., Nordstrom, I. and Hellstrand, P. (2004) Stretch of the vascular wall induces smooth muscle differentiation by promoting actin polymerization. *J. Biol. Chem.*, **279**, 34849–34855.
87. Miyamoto, K., Pasque, V., Jullien, J. and Gurdon, J.B. (2011) Nuclear actin polymerization is required for transcriptional reprogramming of Oct4 by oocytes. *Genes Dev.*, **25**, 946–958.
88. Bligh, E.G. and Dyer, W.J. (1959) A rapid method of total lipid extraction and purification. *Can. J. Biochem. Physiol.*, **37**, 911–917.
89. Li, F., Marchette, L.D., Brush, R.S., Elliott, M.H., Le, Y.Z., Henry, K.A., Anderson, A.G., Zhao, C., Sun, X., Zhang, K. *et al.* (2009) DHA does not protect ELOVL4 transgenic mice from retinal degeneration. *Mol. Vis.*, **15**, 1185–1193.
90. Ford, D.A., Monda, J.K., Brush, R.S., Anderson, R.E., Richards, M.J. and Fliesler, S.J. (2008) Lipidomic analysis of the retina in a rat model of Smith-Lemli-Opitz syndrome: alterations in docosahexaenoic acid content of phospholipid molecular species. *J. Neurochem.*, **105**, 1032–1047.
91. Yu, M., Benham, A., Logan, S., Brush, R.S., Mandal, M.N., Anderson, R.E. and Agbaga, M.P. (2012) ELOVL4 protein preferentially elongates 20:5n3 to very long chain PUFAs over 20:4n6 and 22:6n3. *J. Lipid Res.*, **53**, 494–504.